



Atomistic modeling of physical vapor deposition on complex topology substrates

Michael G. Eberhardt ^a, Andrea M. Hodge ^{a,b}, Paulo S. Branicio ^{a,*}

^a Mork Family Department of Chemical Engineering and Materials Science, University of Southern California, Los Angeles, CA 90089, United States

^b Department of Aerospace and Mechanical Engineering, University of Southern California, Los Angeles, CA 90089, USA



ARTICLE INFO

Keywords:

Molecular Dynamics
Physical Vapor Deposition
Non-flat substrates
Complex topology

ABSTRACT

Molecular Dynamics simulations of Cu physical vapor deposition are employed to investigate the effects of substrate topology and line of sight on the synthesis of thin films on Cu substrates. The deposition and surface relaxation processes of sputtering Cu ions are simulated considering various angles of incidence (0–60°) and sputtering energies (1, 10, 25, and 50 eV). Cu substrates are constructed with three different surface geometries: i) a flat Cu (1 1 1) surface; ii) a sinusoidal shaped substrate with a period of 127.6 Å and amplitude 20 Å, and iii) a combined substrate composed of a flat Cu (1 1 1) surface and a cylinder of radius 63.8 Å, floating 50 Å above the flat surface. Results from simulations with low impact energy (1 eV) show a strong effect of the angle of incidence on the roughness of the thin film produced on the flat surface. For non-flat substrates, areas with no line of sight have diminished film coverage, which is offset by increasing the deposition energy. Higher energy atoms have greater adatom mobility enabling the coverage of regions with no line of sight and the reduction of surface roughness. The results show a lower sticking probability for highly energetic deposition at high angles of deposition, effectively promoting film coverage in areas with no line of sight through physical redeposition processes, which is augmented by particle-induced sputtering. These atomistic insights are relevant for the understanding of physical vapor deposition processes on convoluted topology substrates, such as magnetron sputtering on metamaterial lattices.

1. Introduction

Physical vapor deposition (PVD) has become increasingly prevalent in research and industrial applications in the synthesis of thin film coatings [1–3]. In particular, magnetron sputtering has garnered large interest due to its ability to generate smooth finishes with good mechanical properties at relatively low temperatures [4]. However, the recent increase in the complexity of substrates in terms of size, shape, and structure has posed challenges to the capabilities and understanding of film growth via PVD. Pioneer studies, such as those conducted by Thornton et al. [5–8] in the 1970's and 1980's – which remain the most comprehensive studies of sputtering, related parameters, and stress evolution – focused primarily on flat substrates. However, these studies offer limited insight into the deposition mechanisms and coating uniformity on current convoluted topology substrates, leaving a knowledge gap in understanding coatings of convoluted surfaces. As complex substrates, such as metamaterial lattices produced by additive manufacturing, become more popular, there is a greater need to

understand their coating mechanisms. In this work, we define complex substrates as any substrate with non-flat features with reduced or no line of sight with the deposition flux.

Magnetron sputtering is commonly performed utilizing one or more planar cathode targets, although there may be line of sight limitations depending on the sputtering conditions and the substrate shape. Alternatively, sputtering can be performed utilizing an inverted cylindrical magnetron (ICM) setup [5,9,10]. ICM utilizes a cylindrical hollow cathode target and offers an ideal setup to coat specific geometries such as wires and rods [10–13], because of its inherent 360° line of sight deposition. Nonetheless, the deposition mechanisms of both flat and cylindrical hollow cathodes on complex substrates are not well understood [14]. To understand the fundamental mechanisms dictating the development of thin films on complex substrates, it is important to first examine the capability offered by sputtering using planar targets at coating complex substrates and areas with reduced or no line of sight.

Modeling based on atomistic methods, such as molecular dynamics (MD) and Monte Carlo (MC), has proven to be a viable and helpful tool

* Corresponding author.

E-mail address: branicio@usc.edu (P.S. Branicio).

in the understanding of thin film growth mechanisms by physical vapor deposition [15–20]. MD has been used to explain the dependence of internal stress on film growth and microstructure [21,22], the effects of deposition angle on microstructure generation [23], and void formation during film growth [24]. More importantly, MD experiments have provided the fundamental knowledge and validation needed to model complex substrates. Information such as the dependence of sputter yield and sticking probability on the angle and energy of deposition is needed to model the deposition processes on complex features such as trenches in electronic circuit boards [25]. MD simulations can be used to gather essential information about the deposition processes at the molecular level. Also, the ability of MD to generate realistic results has been validated against experiments [16,20].

Previous experimental [26–28] and modeling [29–33] investigations have explored PVD on non-flat surfaces, such as concave substrates and to a lesser extent, substrates with grooves or cavities. Experiments show that surface preparation and the choice of PVD techniques can result in rather different film coverage and characteristics [26,28]. MD studies have found that PVD factors such as Ar+/Cu+ ratio can affect the Cu coating coverage of trenches as argon promotes migration of atoms along the walls and breaks bridges growing from sidewalls [34]. These studies have typically focused on the coating of trenches and other features such as those found on circuit boards. Coating more complex substrates, such as those currently generated by additive manufacturing, requires further research and provides an opportunity to leverage MD techniques to study coating mechanisms and coating profiles in convoluted topology structures. While much can be learned from the previous investigations on non-flat substrates [26–33], e.g., those with deep trenches, the conclusions from these investigations do not apply directly to the PVD coating of convoluted topology substrates, where large portions of the structure have no line of sight.

In this work, we aim to improve the understanding of the mechanisms and abilities of planar sputtering as it relates to coating complex substrates and areas with no line of sight. We use MD simulations to deposit Cu atoms with specific energies and angles of deposition on three different Cu substrates to determine the effects of substrate geometry and line of sight on the synthesis of thin films. The results show very distinct coatings generated as a function of angle of deposition and energy. In particular, the results indicate that the line-of-sight problem can be largely offset with the use of high energy deposition and non-collimated, i.e., non-zero angle of deposition.

2. Methodology

MD simulations are conducted using LAMMPS [35]. Interatomic forces are calculated using the EAM potential proposed by Mishin et al.

[36]. In all simulations, Cu atoms are deposited on a Face Centered Cubic (FCC) Cu (111) substrate with a 3.61 Å lattice constant. Three different substrates, illustrated in Fig. 1, are used to evaluate the effect of topology. The first substrate is a flat reference model with a size of 127.63 × 110.53 × 37.52 Å placed in an MD simulation box 100.04 Å long along the z-direction. The second substrate is a sinusoidal substrate placed in an MD simulation box 150.06 Å long along the z-direction. The sinusoid runs along the x-axis with a period of 127.63 Å, an amplitude of 20 Å, and a peak position at 75.03 Å. The surface profile and the slope of the structure surface is shown in Fig. S1. The third substrate is composed of two pieces. The first piece is a flat substrate with the same dimensions as the first substrate placed in an MD simulation box 181.33 Å long along the z-direction. Above the flat substrate, a floating cylinder with a radius of 31.98 Å is placed along the periodic y-axis with an x-position of 63.82 Å and a z-position of 87.54 Å. On the bottom of all models, a 3.61 Å of vacuum space is applied along the z-direction. Periodic boundary conditions are applied along the x and y directions in all simulations, while free surfaces are present along the non-periodic z-direction.

The three substrates serve different purposes. The flat model is a reference model to examine the relationships between deposition energy, angle, and surface roughness. It also serves to validate our simulations against previous research. The final application of the flat substrate is to model the film surface on larger substrate features. The substrates examined in this work have features in the nanoscale, while metamaterial lattice struts commonly are in the microscale. Therefore, the flat substrate serves to model a small section of the film developed on these structures. The sinusoidal model addresses deposition with partial line-of-sight and film development on uneven surfaces. Finally, the plane plus cylinder model is a simplification of a metamaterial lattice. It can be seen as an isolated cylindrical unit of a lattice with a planar section to simulate other portions of the structure. A cylinder shape was chosen as common metamaterial lattices, such as Octet-truss, 3D Kagome, and Tetrakaidecahedron, are composed of an array of cylindrical struts [37,38].

All substrates are divided into three regions: *Frozen*, i.e., a region where atoms positions are fixed during the whole simulation; *Thermostat*, i.e., a region where the temperature is controlled by applying a thermostat; *Newtonian*, a region where atoms are free to move according to the calculated forces. The bottom three layers of all substrates are set as the *Frozen* layer. The *Thermostat* and *Newtonian* regions vary by size for the different substrates. However, the *Thermostat* region is always in the middle and is held at 300 K using a Langevin thermostat. The top *Newtonian* layer is 12.50 Å thick for the flat substrate, the flat substrate in the floating cylinder simulation, and the sinusoidal substrate. For the floating cylinder itself, the inner portion with a radius of 7.66 Å is set as a *Frozen* region, and the *Thermostat* region is set as the remaining

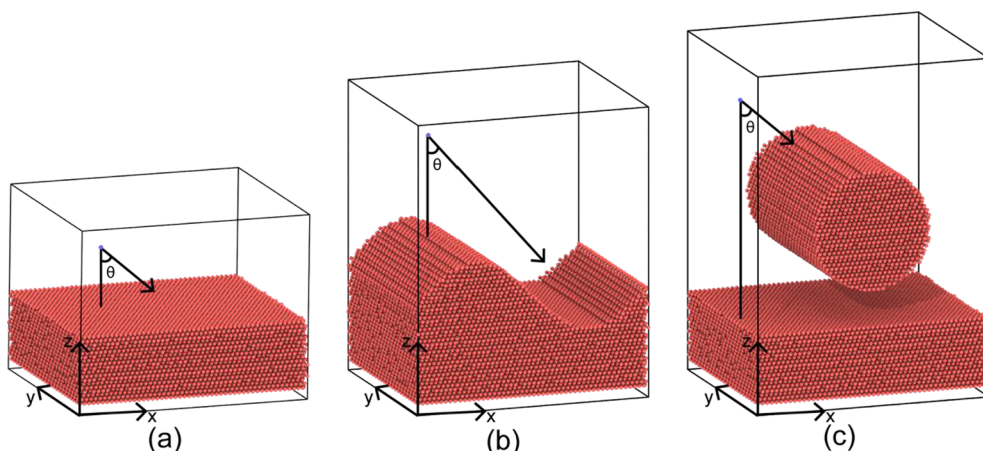


Fig. 1. Simulation models for physical vapor deposition of copper on convoluted copper substrates. (a) flat reference model; (b) sinusoidal model with period 127.6 Å and amplitude 20 Å; (c) flat model with floating cylinder of radius 31.98 Å. Deposition angle is shown in each model.

cylinder within a radius of 20.42 Å. The remaining layers on the outside are set as *Newtonian*.

All simulations use a dynamic time step with a maximum value of 1 fs, which is reduced automatically to ensure atomic motion displacements are less than 0.2 Å per timestep. At the start of all simulations, the various regions are set to the desired temperatures and the system is thermalized until the top *Newtonian* layers have reached a stable temperature of 300 K. The deposition is performed assuming a fixed boundary along the z-direction with a reflective wall set above the deposition region, i.e., the region where sputter atoms are randomly introduced, which is set as a 6.25 Å thick layer on the top z-direction, with an area that spans the entire x and y dimensions of the MD simulation box. An atom at a time is inserted at the set energy and angle of deposition, at a deposition rate of 1 atom per 2,000 timesteps. For the flat substrate dimensions, this deposition rate generates ~0.42 nm/ns of surface coating. To achieve the chosen energy and angle, the particles are assigned velocities along the z and x directions. Each simulation continues until 20,000 particles have been deposited. Once all particles have been deposited, the systems are relaxed for additional 100 ps. Data analysis and visualizations are performed with OVITO [39].

3. Results

Initial simulations on the flat substrate are run to establish a reference to evaluate the effects of deposition angle and energy on the development of thin films on complex substrates as shown in Figs. 2-4. Additional figures for 10 eV simulations can be found in Figs. S2-S4. Fig. 2 shows the surface morphology of thin films developed under deposition energy of 1 eV and deposition angles of (a) 0°, (b) 30°, (c) 45°, and (d) 60° from a plane normal to the surface. The deposited atoms are colored according to their z-position from the substrate surface, while substrate atoms are colored in dark blue. Deposition at 1 eV produces a rough film morphology displaying well-defined peaks and valleys for all deposition angles; although, deposition at lower angles produces a more uniform film coverage. As the deposition angle increases, one can note that peaks and valleys became sharper, i.e., peaks heights are increased while valleys become deeper as the deposition angle increases from 0° to 60°. However, the number of peaks is similar at all angles. As a result, there is a noticeable increase in the surface roughness as the deposition angle increases. As will be discussed, simulations of deposition at higher energies show similar trends.

In Fig. 3 we can see the morphology of the films developed for deposition at different angles and deposition energy of 25 eV. The produced films in this case are all relatively smooth with only a few layers of atoms difference between the highest and lowest atoms of the films, according to their film height values. However, one still can note a slight increase in the film roughness as the angle of deposition increases. The film shown in Fig. 3(a) has no distinct peaks and valleys as there is no pattern in the variation of the surface height. As the angle increases, rather distinct island-like structures become more defined, where

valleys and peaks can be identified.

A similar trend in the film surface morphology as a function of deposition angle is seen for deposition at 50 eV, the highest deposition energy employed, as shown in Fig. 4. In the morphology of the thin films shown in Fig. 4, one can note once again that low deposition angles, i.e., 0° and 30°, result in uniform films with relatively few peaks and valleys. Meanwhile, higher deposition angles, i.e., 45° and 60°, result in the appearance of more distinct peaks. To be noted, deposition at this high energy results in fewer peaks with greater spacing, leading to a less uniform film coverage.

We quantified the differences in surface morphology illustrated in Figs. 2-4 by calculating the surface roughness at each deposition energy as a function of deposition angle, which is shown in Fig. 5. Here the surface roughness is calculated by the arithmetic mean deviation of the surface atoms z-position according to Eq. (1), adapted from Whitehouse [40]:

$$R_a = \frac{1}{N_s} \sum_{i=1}^{N_s} |z_i - z_s| \quad (1)$$

where N_s is the total number of surface atoms, z_i the z position of the i^{th} surface atom, and z_s the average z position of all surface atoms. Atoms with a coordination number 9 or lower are considered surface atoms since atoms in an FCC lattice have a coordination number of 12. Coordination is calculated assuming a 3 Å cutoff radius, which is at the minimum of the radial distribution function, $g(r)$, between the first and second peaks, see Fig. S5. The data shown in Fig. 5 confirms the previous qualitative discussion of the deposition results. For almost all energy levels, there is a positive correlation between the angle of deposition and the surface roughness of the films generated by PVD. Thus, deposition at a higher angle tends to produce rougher film surfaces. The exceptions are the films produced by deposition at 10 and 25 eV and 60°, having comparable or even lower roughness than films produced at 45°. From Fig. 5, we can also observe the trends in surface roughness across energy levels. One can see that low energy deposition (1 eV) produces the roughest films at any deposition angle. Intriguingly, the results indicate no clear trend in the surface roughness as a function of deposition energy. For low deposition angles, 0° and 30°, deposition at 25 eV produce the smoothest surface followed by deposition at 10 eV. For higher angles, 45° and 60°, deposition at 10 eV produces the smoothest surface followed by 25 eV. Surprisingly, the surface roughness of the film produced at 50 eV is higher than at intermediate energies of 10 and 25 eV at all deposition angles. These results established a reference to analyze the effects of deposition angle and energy on the development of thin films in complex substrates.

Moving onto complex substrates, we first evaluate the formation of film coverage over a substrate displaying a sinusoidal surface profile at various deposition angles and energies. Fig. 6 shows the coverage of the sinusoidal substrate at deposition energy of 1 eV. Here, substrate atoms are shown in blue, while deposited atoms are colored by their distance

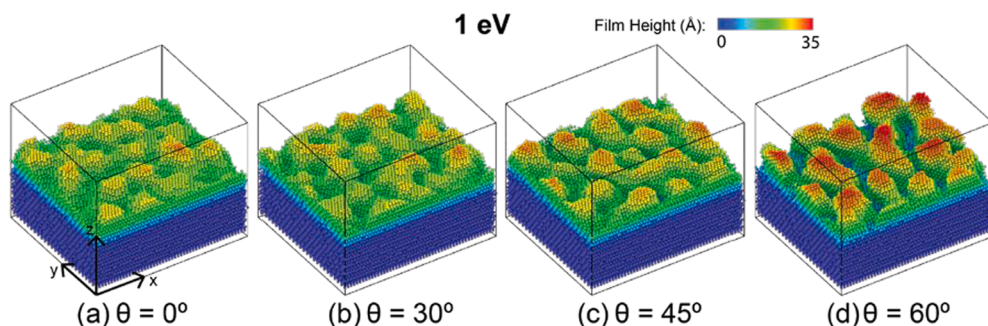


Fig. 2. Surface morphology of copper films deposited at 1 eV at various angles of incidence. (a) $\theta = 0^\circ$; (b) 30° ; (c) 45° ; and (d) 60° . The color of atoms indicates their z position. All substrate atoms are shown as dark blue.

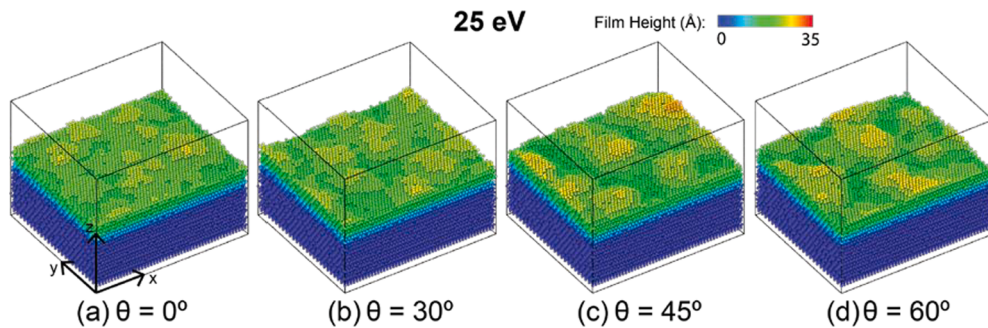


Fig. 3. Surface morphology of copper film deposited at 25 eV at various angles of incidence. (a) $\theta = 0^\circ$; (b) 30° ; (c) 45° ; and (d) 60° . The color of atoms indicates their z position. All substrate atoms are shown as dark blue.

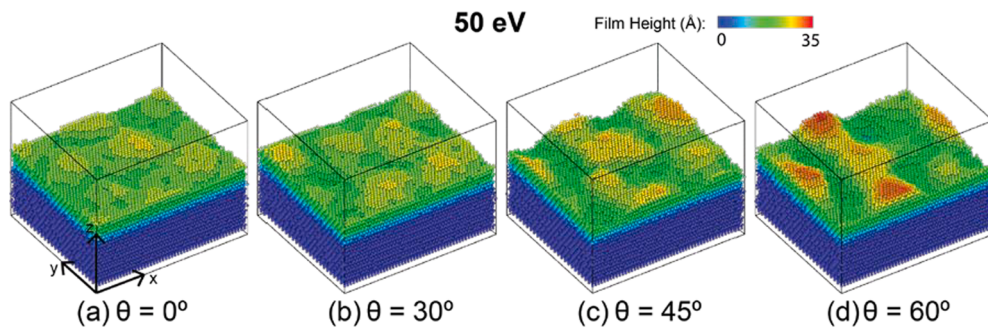


Fig. 4. Surface morphology of copper film deposited at 50 eV at various angles of incidence. (a) 0° ; (b) 30° ; (c) 45° ; (d) 60° . The color of atoms indicates their z position. All substrate atoms are shown as dark blue.

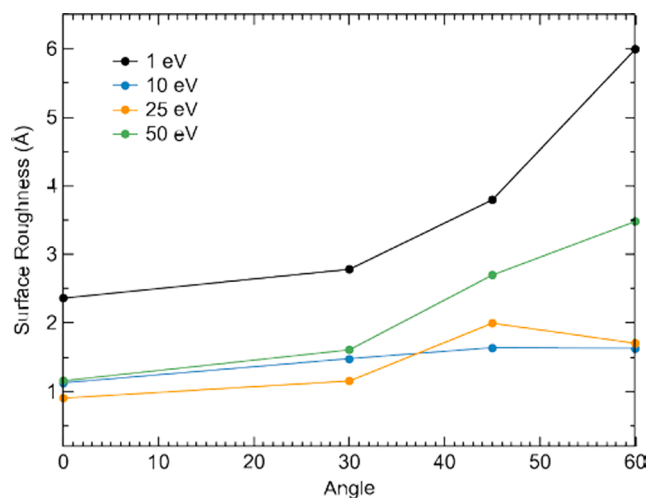


Fig. 5. Surface roughness dependence on angle of deposition.

from the substrate surface along the z -direction. Deposition at 0° , shown in Fig. 6(a), results in a uniform film coverage that conforms to the shape of the substrate. The surface contains peaks and valleys similar to the film produced at 1 eV on the flat substrate. As the angle of deposition increases, the film coverage becomes non-conformal as the fraction of atoms deposited on the downhill portion drastically decreases as the deposition line of sight is reduced. For deposition at 60° , where the slope is completely out of the line of sight, one can note only a few atoms on the slanted slope. To be noted, the film coverage displays sharp edges that generate an overhang at the bottom of the sinusoid. A common trend for the deposition at all angles at this low deposition energy is that deposited atoms are positioned on top of the initial substrate, as no damage is produced to the substrate surface.

Higher deposition energy clearly changes the geometry and coverage of the films produced by PVD as shown in Figs. 7 and 8. Fig. 7 shows films formed by deposition at 25 eV. In contrast with deposition at 1 eV here the data indicates that for all deposition angles, the deposition process displaces some substrate surface atoms, resulting in mixing of substrate and deposited atoms in the film coverage formed, please compare Figs. S11(a)-(d) and Figs. S11(i)-(l). Deposition at 0° results in a reduction of the amplitude of the sinusoidal film in comparison to the sinusoidal substrate surface, as a larger fraction of atoms gather in the bottom of the sinusoid than on the top portion. Increasing the deposition angle once again reduces the fraction of atoms deposited on the downhill surface. However, one can note a larger fraction of atoms deposited on this region than for 1 eV. In addition, the film edges are rounded and there is no longer an overhang produced at 60° deposition angle.

The trends observed for deposition at 25 eV are amplified in the films generated at 50 eV shown in Fig. 8. Figures S11(m)-(p) show that there is a greater mixing of substrate and film atoms as well as visible deeper implantation of sputter atoms in the substrate than for the 25-eV case. One can note a further reduction in the sinusoid amplitude of the film with 0° deposition, as there is an even larger discrepancy in the number of atoms that gather in the bottom of the sinusoid than on the top portion of it. As observed for deposition at 25 eV, as the angle of deposition increases, the fraction of atoms on the downhill surface diminishes. Nonetheless, there is a much larger fraction of atoms on the slanted surface for all deposition angles, as the deposited atoms are able to cover most of the slope – even for deposition at 60° . In addition, the geometry of the film is smooth with no sharp edges or overhangs.

To gain further insight into the development of thin films on complex topologies, we simulate the deposition process using the third model constructed, a floating cylinder model positioned above a flat substrate. In Fig. 9, we can see the pattern of thin film developed by deposition at 1 eV and various angles. The deposited atoms are colored according to their distance from the substrate surface based on whether they are deposited on the cylinder or the flat substrate. The film morphology

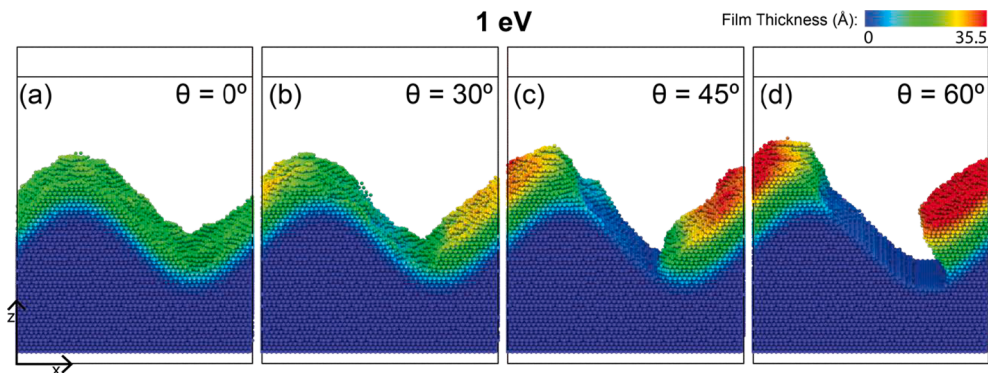


Fig. 6. Coating film development at 1 eV at various angles of deposition for the sinusoidal substrate. Substrate atoms are colored in blue. The color of the atoms indicates the distance from the substrate surface.

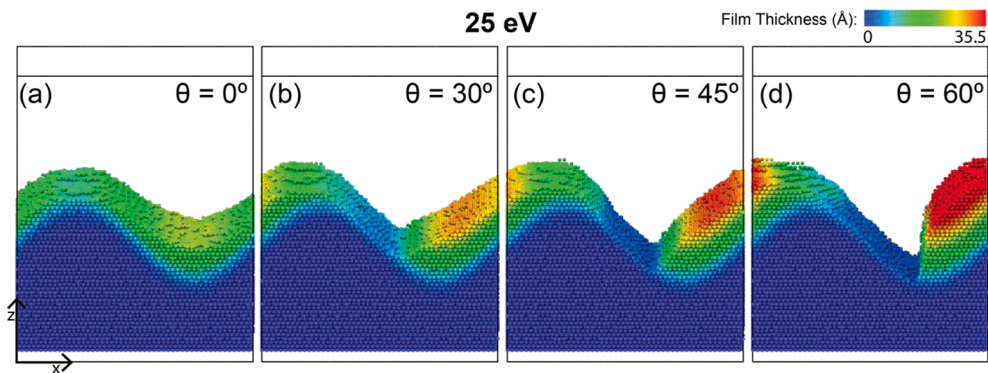


Fig. 7. Coating film development at 25 eV at various angles of deposition for the sinusoidal substrate. Substrate atoms are colored in blue. The color of the atoms indicates the distance from the substrate surface.

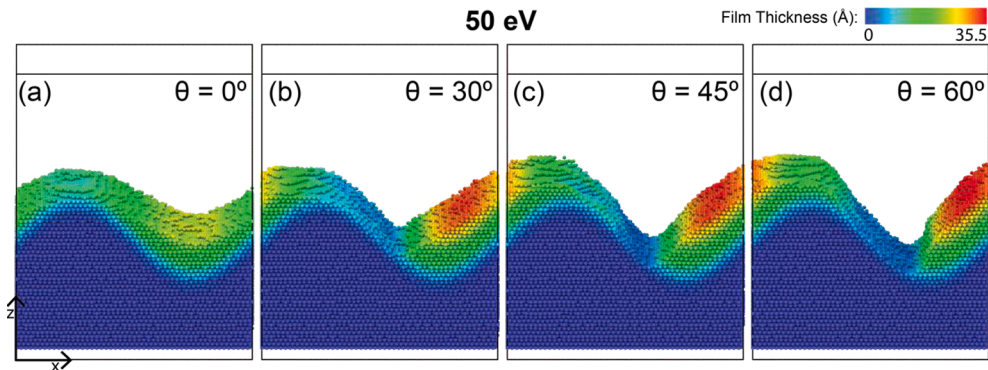


Fig. 8. Coating film development at 50 eV at various angles of deposition for the sinusoidal substrate. Substrate atoms are colored in blue. The color of the atoms indicates the distance from the substrate surface.

shown in Fig. 9 reveals that deposition at 1 eV results in absence of film coverage on areas with no line of sight. For the case of 0° deposition, the deposited atoms build up on top of the cylinder and on areas of the flat substrate with the line of sight not affected by the presence of the cylinder. One can observe that a larger fraction of atoms is deposited on the top center part of the cylinder than on its edges. In addition, no coverage is present on the lower part of the cylinder, which has no line of sight. Changes in the deposition angle result in similar deposition trends, consistent with the change in line of sight. The atoms deposit and stick to regions on the cylinder surface and to areas of the flat substrate that are directly in the line of sight, while there is minimal coverage in other areas. Nonetheless, it is interesting to note that there are a few atoms out of the line of sight, as seen in Fig. 9(b)-(c). Fig. 9d shows the film profile

generated by deposition at 60°. As expected almost all the particles are on the floating cylinder as the line of sight with the substrate is reduced to 0% in the periodic simulation setup used. Only a few particles manage to reach the flat substrate. The deposition of the atoms at this low energy value on the cylinder and flat substrate produces relatively sharp edges for all angles similar to the model with a sinusoidal surface.

As performed for the previous models, we evaluate the effects of high deposition energy in the generated film morphology for the case of the floating cylinder model. The profiles of film coverage at 25 eV are shown in Fig. 10 for various deposition angles. The color coding is the same as the one used in Fig. 9. In contrast with deposition at 1 eV, Fig. 10(a) reveals that deposition at 0° is able to coat a significant portion of the area under the cylinder, with the line of sight blocked by the cylinder,

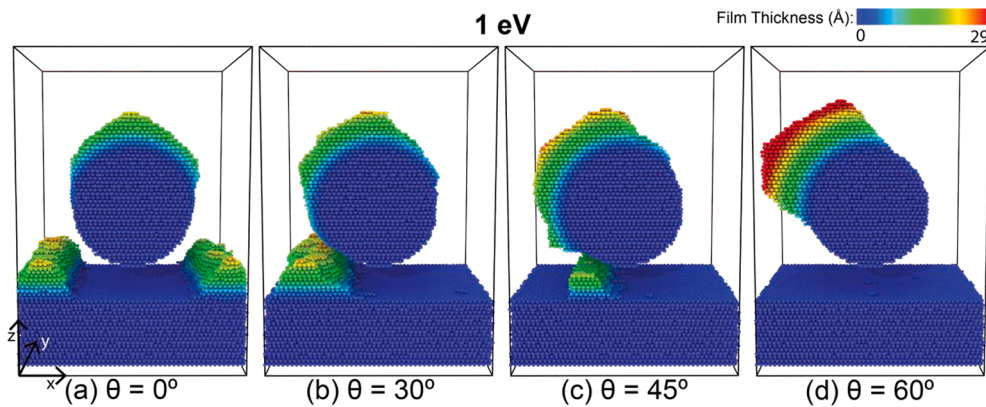


Fig. 9. Coating film development at 1 eV at various angles of deposition for the flat substrate featuring a floating cylinder. Substrate atoms are colored in blue. The color of the atoms indicates the distance from the substrate surface.

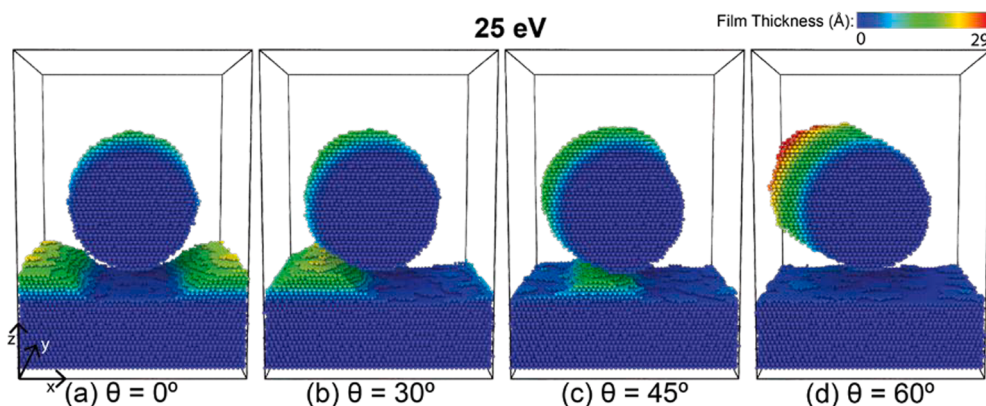


Fig. 10. Coating film development at 25 eV at various angles of deposition for the flat substrate featuring a floating cylinder. Substrate atoms are colored in blue. The color of the atoms indicates the distance from the substrate surface.

with a single layer of atoms. On the cylinder itself, one can note only a thin film coverage formed. However, the coating covers a larger surface area of the cylinder. The coating formed on the substrate is more dispersed and displays smoother edges than for the 1 eV deposition case. Deposition at higher angles results in a similar trend with a thinner film on the cylinder and an increased fraction of atoms deposited on areas without line of sight. One can observe several gaps in the film coverage for deposition at angles different than zero as the formed film is nonuniform. Although it is not visible in the frames shown in Fig. 10, there are atoms present on the lower part of the cylinder for all

deposition angles. Please see supplementary animation Float-25e-0d. It is also important to note that there is an increased mixing of substrate and deposited atoms at this deposition energy level as the atoms are able to penetrate the substrate and displace surface atoms. This results in a film coating that is composed of a mixture of deposited and substrate atoms.

The film morphology trends discussed for deposition at 25 eV can be further seen in the films formed for deposition at 50 eV on the floating cylinder model at various angles shown in Fig. 11. Deposition at 0° results in a very thin coating on the cylinder, which extends around a

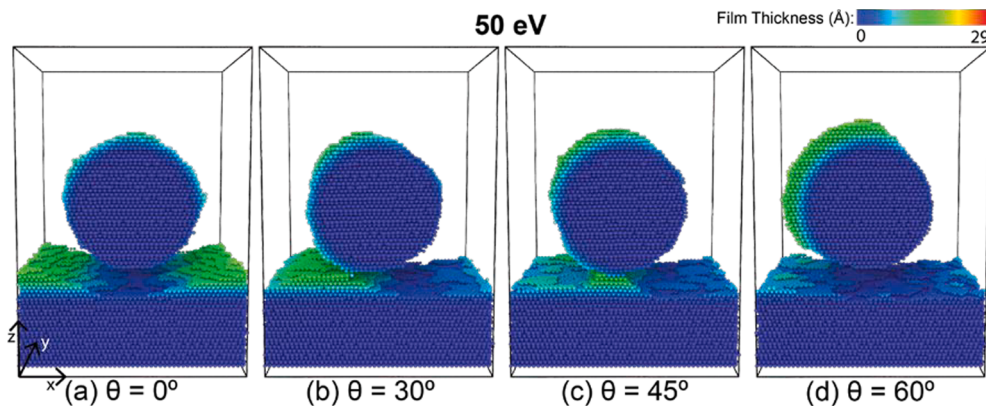


Fig. 11. Coating film development at 50 eV at various angles of deposition for the flat substrate featuring a floating cylinder. Substrate atoms are colored in blue. The color of the atoms indicates the distance from the substrate surface.

greater portion of the cylinder than for deposition at lower energies as previously discussed, please see Fig. 11(a). Coating of the flat substrate at regions with no line of sight is enhanced. Although, one can still note additional buildup and thicker coatings on areas with line of sight. The higher deposition energy also increases the coating coverage on the lower surface of the cylinder forms now an almost complete monolayer leaving only a few uncovered areas. The higher energy also increases the deposition of atoms on the bottom of the cylinder. As the deposition angle is increased a similar pattern of film formation follows. The coating on the cylinder is relatively thinner and more spread than for lower deposition energies, a large fraction of atoms can be found in areas with partial or no line of sight, and the film coverage becomes smoother with fewer sharp edges. The simulation data shows that atoms can be found on the side of the cylinder that is completely shadowed due to the deposition angle, see supplementary animation Float-10e-0d. For deposition at 30° and 45°, at least a monolayer of film coating covers most of the flat substrate with only small gaps in coverage. Meanwhile, deposition at 60°, where the flat substrate is entirely out of the line of sight, still produces a film that covers most of the flat substrate. Some uncovered areas can be found under the cylinder itself (not shown). However, on other areas, multiple layers of atoms are deposited. Once again, the higher energy results in an increased amount of substrate penetration, which damages the surface substrate and causes particle-induced sputtering, see Figs. S12(m)-(p). Overall, the higher energy results in greater coverage of areas with limited or no line of sight. Nevertheless, it can damage the substrate surface and displaces a larger amount of substrate atoms.

4. Discussion

As the popularity of additive manufacturing and metamaterials rises, there is an increased need to understand the coating of complex shaped substrates through PVD. Beyond a printed polymer base, metamaterials fabrication typically requires coating by one of three techniques: atomic layer deposition (ALD), plating techniques, and magnetron sputtering [38]. While ALD and plating techniques are well understood they offer limited choices for deposition materials. Thus, there is an increasing interest in the use of versatile PVD techniques, such as magnetron sputtering, to produce coating films with a variety of different materials on these complex substrates [38]. However, as previously mentioned, the synthesis of films on complex-shaped substrates is not well understood, as previous studies have mostly focused on flat substrates or trenches, such as those present in circuit boards [25,34]. To better understand the development of films on complex substrates such as metamaterials, we make use in this work of simplified models of complex substrates, i.e., the sinusoidal and the floating cylinder models. Those represent the key features of complex substrates, e.g., different non-flat surface shapes such as concave and convex surfaces, and areas with reduced or no line of sight with the deposition flux.

To evaluate the coatings produced on complex substrate models we first use a flat substrate, to be able to determine the fundamental development of films using different PVD conditions, i.e., deposition angle and energy. As previously mentioned, the results show that while there is generally a positive correlation between angle and surface roughness, there is no well-defined trend with the deposition energy, even though deposition at the lowest energy, 1 eV, show the largest surface roughness at each deposition angle, as shown in Fig. 5. The lack of trend for the surface roughness with deposition energy can be explained considering the dependence of the sticking probability on deposition angle and energy. Previous studies using MD simulations have determined the effects of deposition angle and energy on the sticking probability of Cu atoms on Cu substrates [16,29] showing that low angle deposition (less than 20°) results in nearly 100% sticking probability for all energy levels. However, for deposition at higher angles, the sticking probability is highly dependent on the deposition energy. At high angles, the sticking probability for low energy particles

(~1–10 eV) remains around 100% while it is greatly reduced for higher deposition energies. For example, deposition at 50 eV and 60° results in a negligible sticking probability of Cu atoms deposited on a Cu (111) surface [29]. Nonetheless, the sticking probability was shown to be higher on a rough surface [16]. Experimental results using glancing angle deposition show a similar dependence of sticking probability on angle and energy as predicted by MD simulations [41]. The low sticking probability for 50 eV in comparison to the 10 eV and 25 eV simulations help to explain the observed higher surface roughness. The high angle 50 eV deposition results in most atoms bouncing off the substrate surface, particularly for the initial flat Cu (111) surface. The atoms will not settle until they have lost enough energy to stick to the surface after reflecting multiple times or colliding with an existing structure. This results in a reduced effective deposition energy. Another important factor to consider is the particle-induced sputtering of substrate atoms and the resulting increased roughness due to atom displacement. Brief animations are provided in the [supplementary materials](#) highlighting the initial deposition process. Figures S6–S9 highlight the effects of particle-induced sputtering on the floating cylinder model, showing that deposition at higher energies results in a larger number of atoms being ejected from the flat substrate and cylinder and deposited somewhere else. These atoms have much less energy than atoms being deposited and could deposit in a less energetically favorable position resulting in a rougher surface. Incoming particles could also displace atoms of the film that have previously settled on the substrate. This would result in a similar effect but to a greater extent than what is displayed by the displacement of the substrate atoms alone. The flat model shows that sticking probability and redeposition can have a large impact on the development of films, which is magnified for more complex substrates.

The process of uniformly coating complex-shaped objects such as metamaterial lattices to create a uniform film is challenging as there are areas out of the direct line of sight of depositing atoms. However, our results and those of others suggest that effective coating with PVD is possible. From our results, we propose that adatom mobility, sticking probability, redeposition, and particle-induced sputtering are important factors controlling the overall coverage of coating areas with limited or no line of sight. The four factors are reliant on the energy and angle of deposition. As previously discussed, the results show that the use of higher deposition energy tends to produce smoother films as there are smoother edges and a smaller amount of localized build-up. Higher energy deposition also results in a larger number of atoms on the slope of the sinusoid model at high angles as well as at the valley of the sinusoid, see Fig. 8. For the floating cylinder model, high energy leads to enhanced deposition on the flat substrate under the cylinder and on the bottom side of the cylinder itself. These suggest a higher adatom mobility as atoms are able to displace out of the impact site and diffuse across the surface of the substrate. Adatom mobility contributes to coating areas out of the line of sight by locally increasing the diffusion of deposited atoms leading to relaxed and stable coating film structures with reduced surface roughness. This is similar to the coverage of trenches shown in MD simulations conducted by Hwang et al. [34]. They found that argon contributes to complete filling of the trenches in two ways: 1) peeling away atoms from clusters allowing them to migrate down the trenches sidewalls, 2) breaking bridges that form between the sides of the trench [34]. The atoms must migrate once they land in the trench to cover its bottom area, which is analogous to the higher energy atoms moving along the surface onto areas out of the line of sight, such as the sinusoid slope and under the cylinder in our simulations. Higher energy atoms also have a greater chance to disrupt deposited formations similar to argon.

In addition to high deposition energy, redeposition caused by bouncing atoms and particle-induced sputtering is key to coating areas with no line of sight. A low sticking probability leads to a large fraction of depositing atoms bouncing off the surface and redepositing in shadowed regions. The coating of the underside of the floating cylinder aligns with results reported by Juarez et al. [42], where it was observed that

magnetron sputtering was able to coat all sides of a 3D printed polymer micro-truss structure. Nevertheless, the observed coating of the structure on top regions with a direct line of sight, was much thicker than the coating on bottom sections of the material, with no line of sight. **Supplementary Figs. S6-S9** highlight the effect of high deposition energy, i.e., 25 and 50 eV, on the structure of the cylinder and flat surfaces of the composite floating cylinder model. In particular, the figures show that many atoms from the flat substrate are redeposited onto the cylinder surface and vice versa. In contrast, low deposition energy, i.e., 1 and 10 eV, leads to minimal substrate disturbance and thus is not included. The sputtering of these atoms produces a thin film coating of areas that would otherwise be out of the line of sight. As previously mentioned, the quantity of sputtering represented by **Supplementary Figs. S6-S9** is less than the total amount of sputtered atoms as it only represents the initial substrate atoms that are displaced. Once particles have settled in a film, they could also be subject to particle-induced sputtering. This would lead to an even greater number of atoms being displaced from their original location and potentially be able to settle in areas with no line of sight. It is important to note that this increased sputtering is partly the result of an increased amount of damage to the initial substrate as the energy increases. Higher energy deposition tends to slightly affect the initial shape of the substrate as depositing atoms displace substrate atoms. In contrast, during deposition at low energy atoms stick to the areas they land with minimum diffusion out the deposition site and no sputtering.

Another result of this work is the limitation caused by the use of unidirectional deposition for covering both simple and complex substrates. In this work, we purposely use single-angle deposition to evaluate its effect. Results show that deposition at a single angle can result in localized deposition buildup, which leads to an uneven coating thickness or a rougher coating surface. As previously mentioned, changing the angle of deposition changes the area of the substrate that is in the line of sight allowing for coverage of different areas. As a result, atoms tend to accumulate on the areas in the line of sight thus suggesting the need to employ deposition at multiple angles to properly coat the whole surface. Experimentally, this problem is often addressed by either rotating the substrate during the deposition process or by using multiple sources [26,38,42,43]. Karabacak and Lu [43] found that deposition at an angle less than 30° while rotating the substrate produced a more conformal film in a trench than normal deposition. They believe that this is the result of reducing the “shadowing effect,” which essentially puts the side walls in the line of sight.

Another potential limitation of this work is that only one simulation was run for each set up. Nonetheless, while one simulation was run, we expect that further independent runs will produce similar surface roughness values and development of the films.

The synthesis of uniform thin films on complex substrates has been inconsistent, highlighting several challenges. Montemayor et al. [44] were able to produce relatively uniform gold coatings on metamaterials by optimizing sputter conditions. However, it was revealed that the relative density of the metamaterial structure has a strong effect on the degree of film uniformity achievable with optimized deposition conditions, e.g., the integrity of the coating of structures with relative density higher than 0.04 was compromised. It should be mentioned that a metamaterial with a high relative density will result in areas with limited or no line of sight with the sputter flux, even if rotation of substrate or multiples sources are used. In another work, Lontas and Greer [45], struggled to produce an even coating. Our research provides insights into the fundamental behavior of sputtering in the coverage of complex substrates as a function of angle and energy. We show that increased energy can promote coverage in areas out of the line of sight and produce more uniform coverage through redeposition and adatom mobility. However, there is a trade-off as there is an increased amount of damage to the initial substrate as there is a greater amount of penetration.

Further studies should consider the coating of complex substrates

using a combination of multiple angles and energies. In fact, sputter deposition is based on a cosine emission of sputter atoms from the target [46]. The flux of sputter atoms can and is often collimated to improve the quality of produced thin-film coatings [47-49]. However, it is important to consider the possible effect of 360° deposition of complex substrates since that can be related to deposition using a rotating substrate or deposition using a hollow cathode [5,12,27,50,51]. Our results reveal that it is possible to cover areas that are totally shadowed by increasing the deposition energy. However, further research is required to determine the optimal conditions to produce uniform conformal coatings on convoluted topology substrates.

5. Conclusions

In this work, we studied the synthesis of thin films on complex topology substrates by molecular dynamics simulations of physical vapor deposition considering the effects of deposition angle and energy. We evaluated the effect of substrate topology by considering three models: a flat substrate, a substrate with sinusoidal grooves, and a combined substrate composed of a flat surface and a floating cylinder. Results agree with previous studies and provide further insight into development of thin films on complex substrates. Akin to previous studies, the flat substrate results show that low energy and high angle deposition leads to relatively rough surfaces. The results for non-flat substrates agree well with previous investigations of deposition on trenches and limited work on other complex substrates. They support that it is possible to overcome the line-of-sight problem and cover obstructed areas by increasing the deposition energy. However, that can generate damage to the surface of the substrate. We identify the increased adatom mobility and a greater rate of redeposition caused by a lower sticking probability, leading to surface bouncing and particle-induced sputtering, as key factors controlling coating coverage and uniformity. The simulation insights are expected to support further research on the optimization of physical vapor deposition methods towards the production of conformal and homogeneous coatings on 3D complex substrates. This research is particularly relevant for the manufacturing of metamaterials, which frequently requires thin film coating, as well as coating of substrates made using additive manufacturing materials.

Credit authorship contribution statement

Michael G. Eberhardt: Methodology, Software, Validation, Formal analysis, Writing – original draft, Visualization. **Andrea M. Hodge:** Conceptualization, Writing – review & editing. **Paulo S. Brancio:** Conceptualization, Resources, Writing – review & editing, Visualization, Supervision.

Declaration of Competing Interest

The authors declare that they have no known competing financial interests or personal relationships that could have appeared to influence the work reported in this paper.

Acknowledgements

Computation for the work described in this paper was supported by the University of Southern California Center for Advanced Research Computing (carc.usc.edu).

Data Availability

The raw/processed data required to reproduce these findings cannot be shared at this time as the data also forms part of an ongoing study.

Appendix A. Supplementary material

Supplementary data to this article can be found online at <https://doi.org/10.1016/j.commatsci.2021.111111>.

References

- [1] B. Navinšek, P. Panjan, I. Milošev, PVD coatings as an environmentally clean alternative to electroplating and electroless processes, *Surf. Coatings Technol.* 116–119 (1999) 476–487, [https://doi.org/10.1016/S0257-8972\(99\)00145-0](https://doi.org/10.1016/S0257-8972(99)00145-0).
- [2] L.B. Freund, S. Suresh, *Thin Film Materials: Stress, Cambridge University Press, Defect Formation and Surface Evolution*, 2003.
- [3] A.A. Tracton (Ed.), *Coating Technology Handbook, 3rd Editio*, CRC Press, 2005.
- [4] A. Baptista, F.J.G. Silva, J. Porteiro, J.L. Míguez, G. Pinto, L. Fernandes, On the Physical Vapour Deposition (PVD): Evolution of Magnetron Sputtering Processes for Industrial Applications, *Procedia Manuf.* 17 (2018) 746–757, <https://doi.org/10.1016/j.promfg.2018.10.125>.
- [5] J.A. Thornton, V.L. Hedgecock, Tubular Hollow Cathode Sputtering Onto Substrates of Complex Shape, *J Vac Sci Technol.* 12 (1) (1975) 93–97, <https://doi.org/10.1116/1.568631>.
- [6] J.A. Thornton, Influence of Apparatus Geometry and Deposition Conditions on the Structure and Topography of Thick Sputtered Coatings, *J Vac Sci Technol.* 11 (4) (1974) 666–670, <https://doi.org/10.1116/1.1312732>.
- [7] J.A. Thornton, The influence of bias sputter parameters on thick copper coatings deposited using a hollow cathode, *Thin Solid Films.* 40 (1977) 335–344, [https://doi.org/10.1016/0040-6090\(77\)90135-3](https://doi.org/10.1016/0040-6090(77)90135-3).
- [8] J.A. Thornton, High Rate Thick Film Growth, *Annu. Rev. Mater. Sci.* 7 (1) (1977) 239–260, <https://doi.org/10.1146/matsci.1977.7.issue-110.1146/annurev.ms.07.080177.001323>.
- [9] W.D. Gill, E. Kay, Efficient low pressure sputtering in a large inverted magnetron suitable for film synthesis, *Rev. Sci. Instrum.* 36 (3) (1965) 277–282, <https://doi.org/10.1063/1.1719553>.
- [10] M. Ihsan, K. Pourrezaei, Effect of deposition parameters on properties of films deposited on fibers by hollow cathode magnetron sputtering, *J. Vac. Sci. Technol. A Vacuum, Surfaces, Film.* 8 (3) (1990) 1304–1312, <https://doi.org/10.1116/1.576872>.
- [11] C. Esparza-Contro, G. Berthomé, G. Renou, F. Robaut, S. Coindreau, C. Vachey, J. Cambin, M. Mantel, L. Latu-Romain, Microstructures of titanium oxide thin films grown continuously on stainless steel wires by PVD in an inverted cylindrical magnetron: Towards an industrial process, *Surf. Coatings Technol.* 389 (2020) 125643, <https://doi.org/10.1016/j.surcoat.2020.125643>.
- [12] D. Glocker, M. Romach, G. Scherer, J. Eichenberger, J. Lanzafame, Inverted Cylindrical Magnetron Sputtering: Advantages of off-axis alignment of substrates on the deposition of optical coatings, *Vak. Forsch. Und Prax.* 26 (4) (2014) 18–23, <https://doi.org/10.1002/vipr.26.410.1002/vipr.201400558>.
- [13] M. Amberg, J. Geerk, M. Keller, A. Fischer, Design, characterisation and operation of an inverted cylindrical magnetron for metal deposition, *Plasma Devices Oper.* 12 (3) (2004) 175–186, <https://doi.org/10.1080/1051999042000237988>.
- [14] J.E. Greene, Review Article: Tracing the recorded history of thin-film sputter deposition: From the 1800s to 2017, *J. Vac. Sci. Technol. A Vacuum, Surfaces, Film.* 35 (5) (2017) 05C204, <https://doi.org/10.1116/1.4998940>.
- [15] H.M. Urbassek, *Simulation of Sputtering, Nucl. Inst. Methods Phys. Res. B.* 122 (1997) 427.
- [16] C.F. Abrams, D.B. Graves, Cu sputtering and deposition by off-normal, near-threshold Cu+ bombardment: Molecular dynamics simulations, *J. Appl. Phys.* 86 (4) (1999) 2263–2267, <https://doi.org/10.1063/1.371040>.
- [17] S.M. Rossnagel, R.S. Robinson, Monte Carlo model of topography development during sputtering, *J. Vac. Sci. Technol. A Vacuum, Surfaces, Film.* 1 (2) (1983) 426–429, <https://doi.org/10.1116/1.571936>.
- [18] G. Zhu, J. Sun, L. Zhang, Z. Gan, Molecular dynamics simulation of temperature effects on deposition of Cu film on Si by magnetron sputtering, *J. Cryst. Growth.* 492 (2018) 60–66, <https://doi.org/10.1016/j.jcrysgeo.2018.04.002>.
- [19] Y.G. Yang, X.W. Zhou, R.A. Johnson, H.N.G. Wadley, Monte Carlo simulation of hyperthermal physical vapor deposition, *Acta Mater.* 49 (16) (2001) 3321–3332, [https://doi.org/10.1016/S1359-6454\(01\)00139-2](https://doi.org/10.1016/S1359-6454(01)00139-2).
- [20] M.O. Bloomfield, T.S. Cale, Modeling of ionized magnetron sputtering of copper, *Mater. Res. Soc. Symp. - Proc.* 616 (2000) 147–152, <https://doi.org/10.1557/proc-616-147>.
- [21] K.-H. Müller, Stress and microstructure of sputter-deposited thin films: Molecular dynamics investigations, *J. Appl. Phys.* 62 (5) (1987) 1796–1799, <https://doi.org/10.1063/1.339559>.
- [22] C.C. Fang, Stress and microstructure of sputter-deposited thin films: Molecular dynamics simulations and experiment, *J. Vac. Sci. Technol. B Microelectron. Nanom. Struct.* 11 (1993) 2947, <https://doi.org/10.1116/1.586566>.
- [23] L. Dong, R.W. Smith, D.J. Srolovitz, I. Introduction, By Oblique Deposition, 80 (1996).
- [24] R.W. Smith, D.J. Srolovitz, Void formation during film growth: A molecular dynamics simulation study, *J. Appl. Phys.* 79 (3) (1996) 1448–1457, <https://doi.org/10.1063/1.360983>.
- [25] J.D. Kress, D.E. Hanson, A.F. Voter, C.L. Liu, X.-Y. Liu, D.G. Coronell, Molecular dynamics simulation of Cu and Ar ion sputtering of Cu (111) surfaces, *J. Vac. Sci. Technol. A Vacuum, Surfaces, Film.* 17 (5) (1999) 2819–2825, <https://doi.org/10.1116/1.581948>.
- [26] A.-L. Thomann, C. Vahlas, L. Aloui, D. Samelot, A. Caillard, N. Shaharil, R. Blanc, E. Millon, Conformity of aluminum thin films deposited onto micro-patterned silicon wafers by pulsed laser deposition, magnetron sputtering, and CVD, *Chem. Vap. Depos.* 17 (10–12) (2011) 366–374, <https://doi.org/10.1002/cvde.201106936>.
- [27] E. Klawuhn, G.C. D'Couto, K.A. Ashtiani, P. Rymer, M.A. Biberger, K.B. Levy, Ionized physical-vapor deposition using a hollow-cathode magnetron source for advanced metallization, *J. Vac. Sci. Technol. A Vacuum, Surfaces, Film.* 18 (4) (2000) 1546–1549, <https://doi.org/10.1116/1.582382>.
- [28] J. White, C. Tenore, A. Pavich, R. Scherzer, S. Stagon, Environmentally benign metallization of material extrusion technology 3D printed acrylonitrile butadiene styrene parts using physical vapor deposition, *Addit. Manuf.* 22 (2018) 279–285, <https://doi.org/10.1016/j.addma.2018.05.016>.
- [29] D.G. Coronell, D.E. Hansen, A.F. Voter, C.-L. Liu, X.-Y. Liu, J.D. Kress, Molecular dynamics-based ion-surface interaction models for ionized physical vapor deposition feature scale simulations, *Appl. Phys. Lett.* 73 (26) (1998) 3860–3862, <https://doi.org/10.1063/1.122917>.
- [30] A.S. Shumilov, I.I. Amirov, Morphology simulation of the surface subjected to low-energy ion sputtering, *Tech. Phys.* 60 (7) (2015) 1056–1062, <https://doi.org/10.1134/S1063784215070245>.
- [31] X.-Y. Liu, M.S. Daw, J.D. Kress, D.E. Hanson, V. Arunachalam, D.G. Coronell, C.-L. Liu, A.F. Voter, Ion solid surface interactions in ionized copper physical vapor deposition, *Thin Solid Films.* 422 (1–2) (2002) 141–149, [https://doi.org/10.1016/S0040-6090\(02\)00870-2](https://doi.org/10.1016/S0040-6090(02)00870-2).
- [32] V. Hrubý, R. Hrach, Computational simulation of metal ion propagation from plasma to substrates with uneven surfaces, *Vacuum.* 90 (2013) 109–113, <https://doi.org/10.1016/j.vacuum.2012.09.005>.
- [33] H. Huang, G.H. Gilmer, T. Diaz de la Rubia, An atomistic simulator for thin film deposition in three dimensions, *J. Appl. Phys.* 84 (7) (1998) 3636–3649, <https://doi.org/10.1063/1.368539>.
- [34] C.-C. Hwang, G.-J. Huang, J.-G. Chang, S.-P. Ju, Study of argon characteristics in ion physical vapor deposition using molecular dynamics simulation, *J. Appl. Phys.* 91 (6) (2002) 3569–3578, <https://doi.org/10.1063/1.1450032>.
- [35] S. Plimpton, Fast Parallel Algorithms for Short-Range Molecular Dynamics, *J. Comput. Phys.* 117 (1) (1995) 1–19, <https://doi.org/10.1006/jcph.1995.1039>.
- [36] Y. Mishin, M.J. Mehl, D.A. Papaconstantopoulos, A.F. Voter, J.D. Kress, Structural stability and lattice defects in copper: Ab initio, tight-binding, and embedded-atom calculations, *Phys. Rev. B.* 63 (2001), 224106, <https://doi.org/10.1103/PhysRevB.63.224106>.
- [37] L.R. Meza, G.P. Philpot, C.M. Portela, A. Maggi, L.C. Montemayor, A. Comella, D. M. Kochmann, J.R. Greer, Reexamining the mechanical property space of three-dimensional lattice architectures, *Acta Mater.* 140 (2017) 424–432, <https://doi.org/10.1016/j.actamat.2017.08.052>.
- [38] A.R. Garcia-Taormina, A. Alwen, R. Schwaiger, A.M. Hodge, A review of coated nano- and micro-lattice materials, *J. Mater. Res.* 36 (18) (2021) 3607–3627, <https://doi.org/10.1557/s43578-021-00178-6>.
- [39] A. Stukowski, Visualization and analysis of atomistic simulation data with OVITO—the Open Visualization Tool, *Model. Simul. Mater. Sci. Eng.* 18 (1) (2010) 015012, <https://doi.org/10.1088/0965-0393/18/1/015012>.
- [40] D. Whitehouse, *Surfaces and Their Measurement*, Elsevier, 2002. <https://doi.org/10.1016/B978-1-903996-01-0.X5000-2>.
- [41] C. Buzea, K. Kaminska, G. Beydaghyan, T. Brown, C. Elliott, C. Dean, K. Robbie, Thickness and density evaluation for nanostructured thin films by glancing angle deposition, *J. Vac. Sci. Technol. B Microelectron. Nanom. Struct.* 23 (6) (2005) 2545, <https://doi.org/10.1116/1.2131079>.
- [42] T. Juarez, A. Schroer, R. Schwaiger, A.M. Hodge, Evaluating sputter deposited metal coatings on 3D printed polymer micro-truss structures, *Mater. Des.* 140 (2018) 442–450, <https://doi.org/10.1016/j.matdes.2017.12.005>.
- [43] T. Karabacak, T.-M. Lu, Enhanced step coverage by oblique angle physical vapor deposition, *J. Appl. Phys.* 97 (12) (2005) 124504, <https://doi.org/10.1063/1.1937476>.
- [44] L.C. Montemayor, L.R. Meza, J.R. Greer, Design and fabrication of hollow rigid nanolattices via two-photon lithography, *Adv. Eng. Mater.* 16 (2) (2014) 184–189, <https://doi.org/10.1002/adem.201300254>.
- [45] R. Lioras, J.R. Greer, 3D nano-architected metallic glass: Size effect suppresses catastrophic failure, *Acta Mater.* 133 (2017) 393–407, <https://doi.org/10.1016/j.actamat.2017.05.019>.
- [46] A.H. Simon, Sputter Processing, in: *Handb. Thin Film Depos.*, Third Edit, Elsevier, 2012: pp. 55–88. <https://doi.org/10.1016/B978-1-4377-7873-1.00004-8>.
- [47] N. Motegi, Long-thrown low-pressure sputtering technology for very large-scale integrated devices, *J. Vac. Sci. Technol. B Microelectron. Nanom. Struct.* 13 (1995) 1906. <https://doi.org/10.1116/1.587833>.
- [48] S.M. Rossnagel, D. Mikalsen, H. Kinoshita, J.J. Cuomo, Collimated magnetron sputter deposition, *J. Vac. Sci. Technol. A Vacuum, Surfaces, Film.* 9 (2) (1991) 261–265, <https://doi.org/10.1116/1.577531>.
- [49] S.K. Dew, Theoretical and practical aspects of collimated sputtering, *J. Appl. Phys.* 76 (8) (1994) 4857–4862, <https://doi.org/10.1063/1.358444>.
- [50] D.A. Glocker, Principles and applications of hollow cathode magnetron sputtering sources, *Proc. Annu. Tech. Conf. - Soc. Vac. Coaters.* (1995) 298–302.
- [51] S. Muhl, A. Pérez, The use of hollow cathodes in deposition processes: A critical review, *Thin Solid Films.* 579 (2015) 174–198, <https://doi.org/10.1016/j.tsf.2015.02.066>.